Manaswita Kar | Thomas Körzdörfer

Computational high throughput screening of inorganic cation based halide perovskites for perovskite only tandem solar cells

Suggested citation referring to the original publication:
Materials Research Express 7 (2020) 5, Art. 055502 pp. 1 - 10
DOI: https://doi.org/10.1088/2053-1591/ab8c0d
ISSN: 2053-1591

Journal article | Version of record

Secondary publication archived on the Publication Server of the University of Potsdam:
Zweitveröffentlichungen der Universität Potsdam : Mathematisch-Naturwissenschaftliche Reihe 1438
ISSN: 1866-8372
URN: https://nbn-resolving.org/urn:nbn:de:kobv:517-opus4-516831
DOI: https://doi.org/10.25932/publishup-51683

Materials Research Express

PAPER

Computational high throughput screening of inorganic cation based halide perovskites for perovskite only tandem solar cells

M Kar[1] and T Körzdörfer[2]

[1] Department of Engineering Materials, University of Southampton, United Kingdom
[2] Institute of Chemistry, University of Potsdam, Germany

E-mail: M.Kar@soton.ac.uk

Keywords: inorganic perovskites, tandem solar cells, density functional theory

Supplementary material for this article is available online

OPEN ACCESS

RECEIVED
31 March 2020

REVISED
16 April 2020

ACCEPTED FOR PUBLICATION
22 April 2020

PUBLISHED
4 May 2020

Abstract

We search for homovalent alternatives for A, B, and X-ions in ABX_3 type inorganic halide perovskites suitable for tandem solar cell applications. We replace the conventional A-site organic cation CH_3NH_3, by 3 inorganic cations, Cs, K, and Rb, and the B site consists of metals; Cd, Hg, Ge, Pb, and Sn This work is built on our previous high throughput screening of hybrid perovskite materials (Kar *et al* 2018 *J. Chem. Phys.* **149**, 214701). By performing a systematic screening study using Density Functional Theory (DFT) methods, we found 11 suitable candidates; 2 Cs-based, 3 K-based and 6 Rb-based that are suitable for tandem solar cell applications.

1. Introduction

Halide perovskites in general and hybrid halide perovskites in particular have gained importance in the photovoltaics market for many years, especially because of the rapid power conversion efficiency achieved by these perovskite solar cells over a very short span of research time. Low processing cost and abundant available raw materials allows easy fabrication of these materials, thus making them a potentially competitive alternative to the massively used silicon solar cells in terms of commercialization [1–3]. Conventionally, the most important member of the halide perovskites family is the methylammonium lead iodide, $CH_3NH_3PbI_3$, which was discovered by Dieter Weber in 1978 [4] and was first used for photovoltaic application by Kojima *et al* in 2009 [5]. The highest power conversion efficiency recorded so far by a single junction solar cell device made of $CH_3NH_3PbI_3$ is 22.1% in 2015 by Park *et al* [6]. In 1980, following the detailed balance limit principle of single p-n junction solar cell devices [7], Alexis De Vos came up with the idea of the fundamental detailed balance limit for a tandem solar cell [8]. According to this paper, promising efficiencies can be achieved if two single junction solar cell devices with specifically tailored band gaps are combined to form a two-junction tandem solar cell. For instance, efficiency of 42.3% can be achieved, in theory, by two single junction solar cell devices of band gaps 1.0 eV and 1.9 eV respectively.

So far, the maximum efficiency achieved by inorganic tandem solar cells has been recorded to be about 32.8% for unconcentrated GaInP/GaAs monolithic 2-junction, 2-terminal device, and 35.5% for 2-junction, 2-terminal tandem GaInAsP/GaInAs concentrator cell [9, 10]. The maximum efficiency of perovskite/Si monolithic tandem solar cell is 23.6% as recorded so far [10]. This far, to the best of our knowledge, there has been no experimental literature that explored the prospects of tandem solar cell efficiencies based on hybrid halide perovskites. There are, however, a number of theoretical publications available, that concentrated in high- throughput screening of perovskite materials, in terms of their energy band gaps using density functional theory calculations [11–22]. In 2018, we performed a high-throughput study on hybrid perovskite materials based on DFT calculations that aimed in finding novel perovskite materials for hybrid perovskite-only tandem solar cells [23]. We came up with 8 hybrid perovskites, 5 of which are in the lower band gap range and 3 in the higher band gap range.

One of the major challenges faced by these perovskite materials is the stability issue. Hybrid perovskites have low thermal decomposition temperature which is mainly due to the presence of the unstable organic monovalent cations [24–28]. This instability poses a major challenge towards understanding the fundamental

Table 1. The ionic radii of the inorganic cations and the halogen ions used for the GTF calculation.

Element	Atomic radius (pm)
Rb^{+}	152
K^{+}	138
Cs^{+}	167
Cd^{2+}	95
Ge^{2+}	73
Pb^{2+}	119
Hg^{2+}	102
Sn^{2+}	118
Cl-	184
Br-	196
I-	220

mechanism of how these perovskites work. More importantly, many abnormal phenomena have been found while exploring these perovskite materials. Inorganic materials are known to have higher stability than the organic materials, especially at higher temperatures [29–31]. This aspect has been exploited quite well experimentally, in which the organic cation has been replaced by the inorganic Cs^{+} cation that resulted in a rapid decrease in instability problems, thereby promising a relatively higher intrinsic or thermodynamic stability against decomposition to binary halide products [32–44]. However, theoretical investigation towards this pressing issue is still limited [11–19].

In this paper, we aim at replacing the organic cation in the hybrid perovskites by inorganic cations bearing similar oxidation state as CH_3NH_3. The organic cations that are selected to be potential replacement of CH_3NH_3 must also have a comparable ionic radius. However, the calculation of the ionic radius of CH_3NH_3 proves to be challenging. Two groups have worked towards this problem using different methods [45, 46]. In 2014, Amat *et al* calculated the radius of the methylammonium cation by calculating the volume inside a contour of 0.001 electrons/$Bohr^3$ density, and came out with a value of 2.70 Å [47]. Kieslich *et al* [48] considered a hard sphere model in which the cation rotates freely about it's center of mass. This method yielded a value of 2.17 Å. It is well established by now, that the empirical stability of the hybrid perovskites are calculate using the Goldschmidt tolerance factor, a value that is dependent on the atomic radii of the A-site cation, the metal, and the halogen. It is also well known that two classic perovskites $CH_3NH_3PbBr_3$ and $CH_3NH_3PbCl_3$ adopt the ideal cubic perovskite structure, i.e. the tolerance factor must lie between 0.9 and 1.0. Considering that the ionic radii of Pb, Br, and Cl are 1.19 Å, 1.96 Å, and 1.81 Å, respectively, the radius of methylammonium cation should lie between 2.04 Å and 2.50 Å. Therefore, 2.17 Å is considered to be the more agreeable value for the methylammonium cation [47, 48].

In this study, we replace the methylammonium cation with 3 inorganic cations: Rb+, Cs+, and K+. The respective ionic radii are provided in table 1. A previous study performed by us on hybrid perovskites [23], showed that among 10 metals used in combination with methylammonium and the 3 halogens, only 5 metals, (Cd, Hg, Pb, Sn, and Ge) resulted in perovskites that gave band gaps in the range desired for application in tandem solar cells. Therefore, in this study, we consider only these 5 metals for simulation of the perovskites. The metals, inorganic cations, and the halogens considered in this study are highlighted in figure 1. From our study, we found 11 perovskite materials that proved to be suitable for application in tandem solar cells.

2. Computational details

The calculations on the inorganic perovskites are done using Density Functional Theory (DFT) method using the Fritz-Haber Institute *Ab-initio* Molecular Simulations (FHI-AIMs) software package, developed by the Fritz-Haber Institute, Berlin [42]. We started with 45 perovskite materials, combining 3 inorganic cations, 5 metals, and 3 halogens, as shown in figure 1. The geometry of the perovskites are optimised in all the 3 phases (cubic, orthorhombic, and tetragonal) using the PBE exchange-correlation functional [43] in order to get the structures with the lowest potential energy. The initial lattice parameters of the perovskites are given in supplementary information *is available online at* stacks.iop.org/MRX/7/055502/mmedia. The band gaps of the optimised perovskites are calculated, first using the PBE functional. This functional is less expensive in terms of computational time but is also less accurate for calculating the band gaps of solids. Thus, this functional is used as a pre-screening criterion to find perovskite materials whose band gaps lie in the range of 0.5 eV and 2.5 eV. The band gaps of the perovskites that passed the pre-screening are further calculated, this time using the more accurate but also computationally more expensive HSE functional [49]. All the calculations are done using the

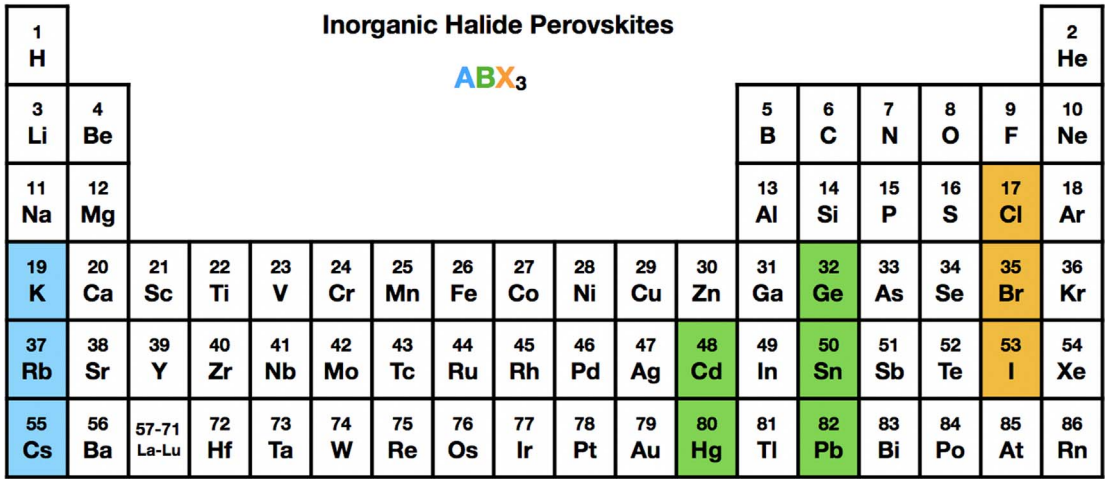

Figure 1. The inorganic cations, the metals, and the halogens used in the study are highlighted in blue, green, and orange, respectively.

spin–orbit coupling corrections because of the heavy elements present in the system [50]. A k-point grid of $3 \times 3 \times 3$ is used for the geometry optimisation and $6 \times 6 \times 6$ grid is used for band gap calculation. All parameters have been tested for convergence.

3. Results and discussions

3.1. Structural and phase stability

The structural and thermodynamic stability of the perovskites is an important aspect to look at, in order to use them for suitable practical applications. Inorganic halide perovskites, in general, are more stable than their hybrid counterparts, the instability of which are owed to the weakly bonded soft organic cation [32–44]. However, the degree of stability varies with the variation of the 3 inorganic cations using in this study.

From the experimental point of view, as mentioned in literature [51, 52], Cs-based halide perovskites are expected to exist in 4 phases: the cubic ($\propto$), the tetragonal (β), and 2 orthorhombic phases (black γ and a non-perovskite yellow δ phase). The cubic ($\propto$) phase is stable at high temperature (>578 K). Upon being cooled down to room temperature, the materials undergo a phase transition to the β and γ phases. These phases, however are thermodynamically not very stable. At room temperature, the materials tend to form the non-perovskite δ phase. The detailed stability of the K- and the Rb- based halide perovskites have not yet been reported.

The structural stability of the inorganic halide perovskites for different phases are determined by calculating their DFT total energies. It is important to note that the DFT total energies are enough to determine the 0 K phase stabilities, which could potentially be different from their room temperature phase stabilities [53, 54]. The 0 K phase stabilities of the inorganic perovskites relative to the cubic phase are shown in figures 2(a)–(c) respectively, for the Rb-, K-, and Cs- based perovskites.

The 0 K total energy calculations of the perovskites do not show any clear trend for the different inorganic cations or for the different halogens. In order to get a more distinct idea about these phase stabilities, we determine the Goldschmidt tolerance factor (GTF) for these perovskites. This is an empirical factor that is used to analyse the phase stability of the perovskites from the radii of the constituent cations and anions. The ionic radii used for the tolerance factor calculation are listed in table 1. The Goldschmidt tolerance factor is calculated as follows [55, 56]:

$$t = (r_A + r_X)/\sqrt{2}(r_B + r_X) \quad (1)$$

Here, r_A, r_B, and r_X are the radii of the inorganic cation, the metal cation and the halogen ion respectively. A value of the GTF between 0.9–1.0 depicts a pure cubic perovskite. Values less than 0.9 or greater than 1.0 depict less symmetric orthorhombic/rhombohedral or tetragonal/hexagonal phases respectively.

The stable phases as obtained from the DFT total energy calculation and the Goldschmidt tolerance factor estimation is shown in table 2. As is seen from table 2, the 0 K phase stability and the empirically predicted room temperature phases of the perovskites are different in most of the cases. This is expected, as the perovskites essentially undergo a phase transition with the change in the temperature. For CsMI3, (M = Pb, Sn) both the 0 K and room temperature stable phases are seen to be orthorhombic. This is at par with what is reported in literature, as already discussed previously. For the remaining perovskites, experimental reports regarding the phases are not available yet.

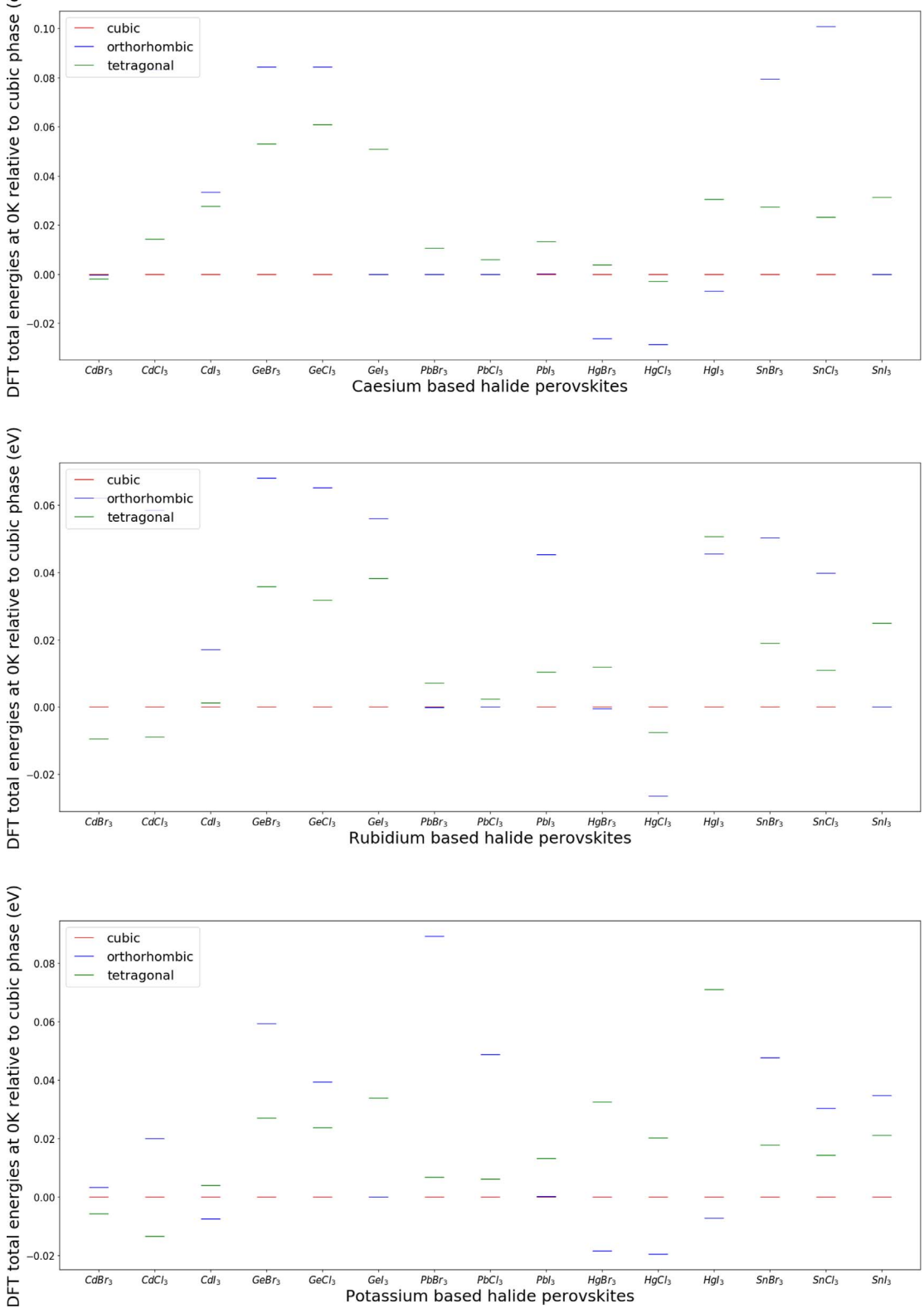

Figure 2. (a): The depiction of phase stability of Cs-based halide perovskites as obtained from DFT total energies. Color coding as shown in legend. (b): The depiction of phase stability of Rb-based halide perovskites as obtained from DFT total energies. Color coding as shown in legend. (c): The depiction of phase stability of K-based halide perovskites as obtained from DFT total energies. Color coding as shown in legend.

3.2. Band structure and band gap

Given that the main aim of our study is to find suitable candidates for tandem solar cells, one of the important characteristic features to look at is the energy band gap of these perovskite materials. The range of band gaps for the most potential candidates is 1.0 eV and 1.9 eV, as already mentioned in the detailed balance limit for tandem cells

Table 2. The stable phases of the inorganic perovskites based on the DFT total energies (0 K) and empirical GTF calculation (room temperature).

Perovskite	GTF	R.T. Stable phase (GTF)	0 K Stable phase (DFT)
CsCdBr3	0.88	Orthorhombic	Tetragonal
CsCdCl3	0.89	Orthorhombic	Cubic
CsCdI3	0.87	Orthorhombic	Cubic
CsGeBr3	0.95	Cubic	Cubic
CsGeCl3	0.96	Cubic	Cubic
CsGeI3	0.93	Cubic	Cubic/ Orthorhombic
CsPbBr3	0.81	Orthorhombic	Cubic/ Orthorhombic
CsPbCl3	0.82	Orthorhombic	Cubic/ Orthorhombic
CsPbI3	0.80	Orthorhombic	Cubic/ Orthorhombic
CsHgBr3	0.86	Orthorhombic	Orthorhombic
CsHgCl3	0.87	Orthorhombic	Orthorhombic
CsHgI3	0.85	Orthorhombic	Orthorhombic
CsSnBr3	0.82	Orthorhombic	Cubic
CsSnCl3	0.82	Orthorhombic	Cubic
CsSnI3	0.80	Orthorhombic	Cubic/ Orthorhombic
RbCdBr3	0.84	Orthorhombic	Tetragonal
RbCdCl3	0.85	Orthorhombic	Tetragonal
RbCdI3	0.83	Orthorhombic	Cubic
RbGeBr3	0.91	Cubic	Cubic
RbGeCl3	0.92	Cubic	Cubic
RbGeI3	0.90	Cubic	Cubic
RbPbBr3	0.78	Orthorhombic	Orthorhombic/ Cubic
RbPbCl3	0.78	Orthorhombic	Orthorhombic/ Cubic
RbPbI3	0.77	Orthorhombic	Cubic
RbHgBr3	0.82	Orthorhombic	Orthorhombic
RbHgCl3	0.83	Orthorhombic	Orthorhombic
RbHgI3	0.81	Orthorhombic	Cubic
RbSnBr3	0.78	Orthorhombic	Cubic
RbSnCl3	0.79	Orthorhombic	Cubic
RbSnI3	0.78	Orthorhombic	Orthorhombic/ Cubic
KCdBr3	0.81	Orthorhombic	Tetragonal
KCdCl3	0.81	Orthorhombic	Tetragonal
KCdI3	0.80	Orthorhombic	Orthorhombic
KGeBr3	0.88	Orthorhombic	Cubic
KGeCl3	0.89	Orthorhombic	Cubic
KGeI3	0.86	Orthorhombic	Cubic
KPbBr3	0.75	Orthorhombic	Cubic
KPbCl3	0.75	Orthorhombic	Cubic
KPbI3	0.75	Orthorhombic	Cubic
KHgBr3	0.79	Orthorhombic	Orthorhombic
KHgCl3	0.79	Orthorhombic	Orthorhombic
KHgI3	0.78	Orthorhombic	Orthorhombic
KSnBr3	0.75	Orthorhombic	Cubic
KSnCl3	0.75	Orthorhombic	Cubic
KSnI3	0.75	Orthorhombic	Cubic

by De Vos in 1980 [8]. In this study, the band gaps of the perovskites in all the 3 phases (orthorhombic, tetragonal, and cubic) are calculated using DFT semi-local PBE and the hybrid HSE functionals. However, as known, the computational calculations come with certain inaccuracies, in order to be safe, we keep a margin of 0.5 eV on both the high and the low ends, i.e. we consider all those perovskites that have a band gap between 0.5 eV and 2.5 eV. The band gaps of the materials are initially calculated using the PBE functional. This functional is computationally less

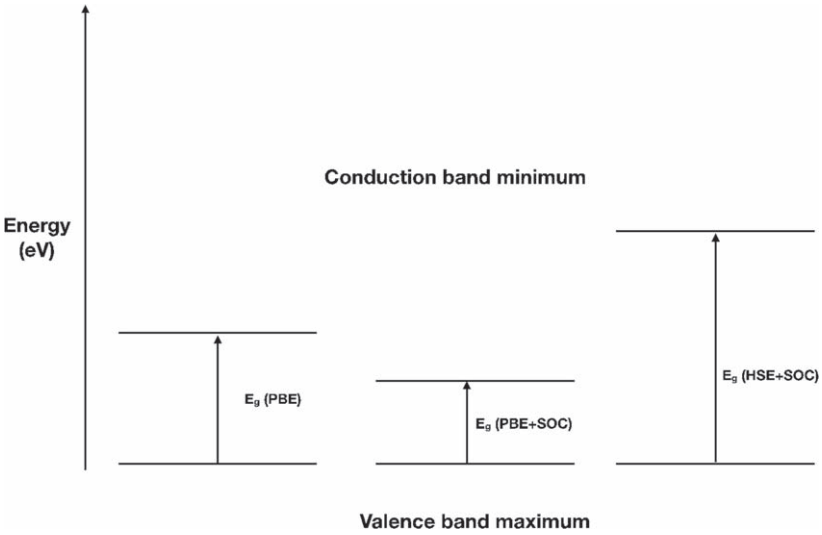

Figure 3. Pictorial depiction of change in the DFT band gaps with the 2 different functionals (PBE and HSE) without and with spin-orbit coupling.

Table 3. The energy band gaps of the room temperature stable phases of the perovskites as predicted by DFT using the HSE functional.

Material	Phase	HSE band gap (eV)
RbCdI3	Orthorhombic	1.91
RbGeBr3	Cubic	1.89
RbHgCl3	Orthorhombic	1.94
RbHgI3	Orthorhombic	2.07
RbSnI3	Orthorhombic	0.98
KGeCl3	Orthorhombic	2.24
KPbBr3	Orthorhombic	2.30
KHgBr3	Orthorhombic	1.90
KHgCl3	Orthorhombic	2.27
KHgI3	Orthorhombic	1.58
KSnBr3	Orthorhombic	1.49
KSnCl3	Orthorhombic	2.47
KSnI3	Orthorhombic	1.14
CsCdI3	Orthorhombic	1.93
CsHgBr3	Orthorhombic	2.33
CsSnI3	Orthorhombic	0.94

expensive, but also less accurate in terms of calculating band gaps of complex periodic materials. Because of this fact, the PBE functional is used as a pre-screening criterion in order to find materials whose band gaps are in the required range. For the materials that pass the pre-screening criterion, the band gaps are again calculated, this time using the more accurate, but also the more computationally expensive hybrid functional, HSE. This functional is thus used for screening the materials to get band gaps in the desired range. It is important to note here that the band gap calculations are done using the spin–orbit coupling, because of the presence of heavy elements in the system. The application of spin–orbit coupling reduces the band gap by a certain amount. Although the precise amount of reduction cannot be estimated, it is found that the band gap is reduced the least for Cl-based perovskites, and the most with I-based perovskites. Based on this observation and from literature findings, it can be inferred that as the halide size increases, the valence band maximum of the perovskite is shifted upwards by the application of spin–orbit coupling. The change in the DFT band gaps of the different perovskites with the 2 different functionals and with and without the application of spin–orbit coupling is shown in figure 3.

The perovskite materials that pass the HSE screening based on their estimated band gaps are listed in the supplementary information. Keeping in mind that the experimental synthesis of these materials are done at room temperature, it is important to correlate the room temperature stable phase with the suitable band gaps. Therefore, we list all those materials that give desired HSE band gaps in the room temperature stable phase in table 3. Finally, it is important to note that for application in photovoltaics, the predicted energy gaps must be

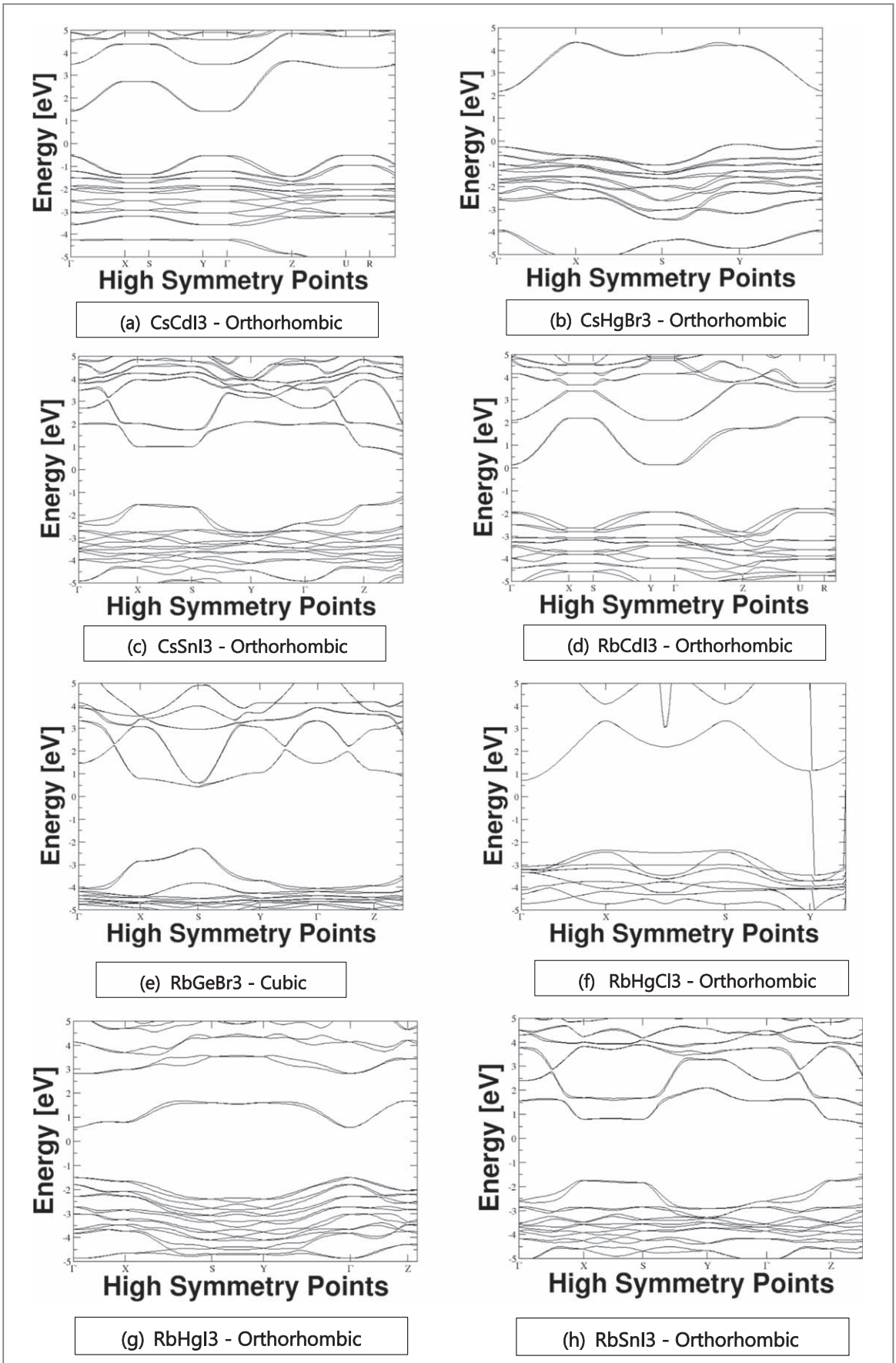

Figure 4. Pictorial depiction of change in the DFT band gaps with the 2 different functionals (PBE and HSE) without and with spin-orbit coupling.

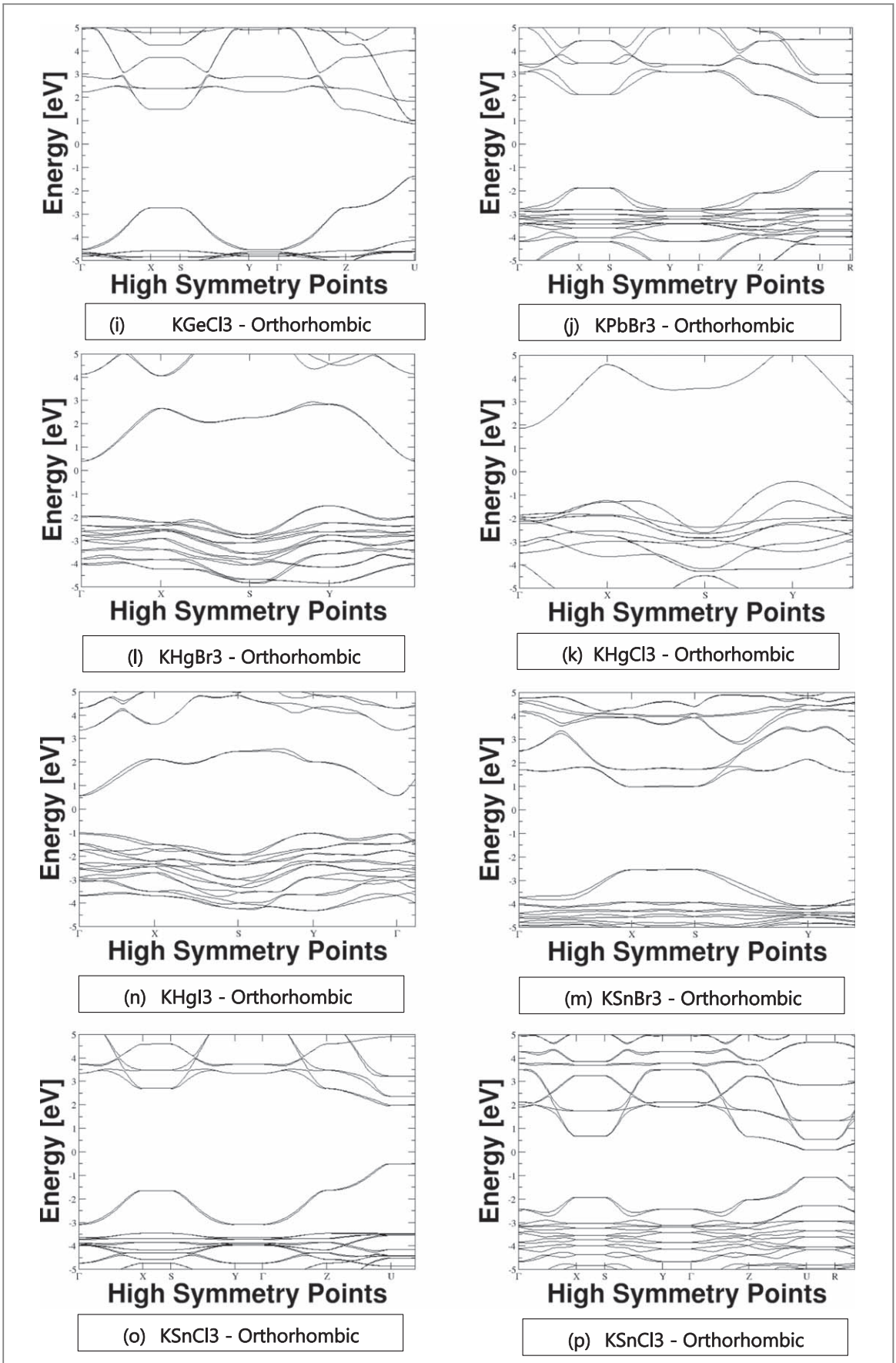

Figure 4. (Continued.)

Table 4. Experimental band gaps of the perovskites as available in literature.

Material	Experimental stable phase	Exp. band gap	References
RbGeBr3	Trigonal	2.74	[38]
CsGeBr3	Trigonal	2.32	[37]
CsGeCl3	Trigonal	3.4	[37]
CsGeI3	Trigonal	1.53	[37–39]
CsSnBr3	Cubic	1.75	[36]
CsSnCl3	Monoclinic	2.8	[37]
CsSnI3	Orthorhombic	1.27	[36]

direct in nature. The nature of the band gaps are understood by plotting the band structures of the materials. The band structures of all the perovskites listed in table 3 are plotted in figure 4. It is observed that Hg on the B-site results in an indirect band gap.

However, an exception exists in case of RbHgI3, in which case, there is a direct band gap at the ðš^{a}-point. From the final step of screening, we obtained 11 perovskite materials; 2 Cs-based, 3 Rb-based, and 6 K-based.

The available experimental band gaps of the perovskites are given in table 4 [35–39]. Upon comparing with the predicted DFT data, it is seen that the band gaps are quite different. This is due to a number of reasons. Firstly, for most of the cases, the experimental and the simulated phases are different, leading to different lattice parameters, lattice angles and bond lengths. The second important reason is that the type of band gaps obtained from the DFT study are different from the ones measured experimentally, the difference between the two being the exciton binding energy and the derivative discontinuity, which is a property of the functional. This is called the band gap problem in DFT and is explained in detail in reference [57].

4. Conclusions

From this study, a number of novel perovskite materials are found those can be used for photovoltaic applications. A few of these materials have already been synthesised and their experimental band gaps are given in table 4. $CsSnBr_3$ and $CsSnI_3$ have PCE of 2.1% and 3.4% respectively in single junction devices [33]. $CsGeI_3$ has a PCE of 0.11% [58]. It is concluded that Ge based perovskites have really low PCE as compared to other metals. However, the PCE of $RbGeBr_3$ is not available. No experimental evidence of the synthesis of Potassium based halide perovskites has been found. But, it can be seen from the DFT studies done here, that these perovskites show promising band gaps as well to be used in photovoltaic devices.

Acknowledgments

The authors thank the HyPerCells graduate school, within the University of Potsdam, for giving the opportunity, as well as the necessary funding to support the project. An award of computation time was provided by the Innovative and Novel Computational Impact on Theory and Experiment (INCITE) program. The research used resources of the Argonne Leadership Computing Facility, which is a DOE Office of Science User Facility supported under Contract No. DE-AC02-06CH11357.

Additional information

The supplementary information containing the results of all the relaxation parameters and the PBE band gaps is available. The necessary computational files are made available in the NOMAD repository.

ORCID iDs

M Kar https://orcid.org/0000-0002-5859-8821

References

[1] Kar M *et al* 2018 *J. Chem. Phys.* **149** 214701
[2] Lee K *et al* 2015 *Light: Sci. Appl.* **4** e288
[3] Alsema E A 2000 *Prog. Photovoltaics Res. Appl.* **8** 17

[4] Palz W *et al* 1991 *Int. J. Sol. Energy* **10** 211
[5] Weber D 1978 *Z. Naturforsch.* **33b** 1443–5
[6] Miyasaka T *et al* 2009 *J. Am. Chem. Soc.* **131** 17
[7] Yang W S *et al* 2017 *Science* **356** 6345
[8] Shockley W *et al* 1961 *J. Appl. Phys.* **32** 3
[9] Vos A D 1980 *J. Phys. D: Appl. Phys.* **13** 839
[10] Green M A *et al* 2018 *Prog. Photovolt. Res. App.* **26** 51
[11] Green M A *et al* 2019 *Prog. Photovolt. Res. App.* **27** 53
[12] Yang W *et al* 2019 *Energy and Environ. Sci.* **12** 2233
[13] Filip M R *et al* 2016 *J. Phys. Chem.* C **120** 1
[14] Sawada K *et al* 2017 *J. Phys. Chem. Lett.* **8** 19
[15] Lu S *et al* 2018 *Nat. Commun.* **9** 3405
[16] Perez R *et al* 2015 *Chem. Mater.* **27** 17
[17] Körbel S *et al* 2018 *J. Mater. Chem.* A **6** 6463
[18] Ono L K *et al* 2017 *ACS Appl. Mater. Interfaces*, **9** 36
[19] Nakajima T *et al* 2017 *J. Phys. Chem. Lett.* **8** 19
[20] Jørgensen P *et al* 2018 *J. Chem. Phys.* **148** 241735
[21] Nagasawa S *et al* 2018 *J. Phys. Chem. Lett.* **9** 2639
[22] Chen F-C 2019 *Int. Jour. Of Polymer Sci.* **2019** 4538514
[23] Jain D *et al* 2019 *Phys. Chem. Chem. Phys.* **21** 19423
[24] Zhao Y *et al* 2019 *Energy Environ. Sci.* **12** 1495
[25] Tai Q *et al* 2019 *Energy Environ. Sci.* **12** 2375
[26] Meng Y *et al* 2019 *Organic Electronics* **64** 47–53
[27] Juarez-Perez E *et al* 2008 *J. Mat. Chem.* A **6** 9604
[28] Dualeh A *et al* 2014 *Chem. Mat.* **26** 21
[29] Brunetti B *et al* 2016 *Scientific Reports* **6** 31896
[30] Kim N-K *et al* 2017 *Scientific Reports* **7** 4645
[31] Qian X *et al* 2016 *Appl. Phys. Lett.* **108** 063902
[32] Krishnamoorthy T *et al* 2015 *J. Mat. Chem.* A **3** 23829
[33] Kim H-S *et al* 2012 *Scientific Reports* **2** 591
[34] Qian J *et al* 2016 *Organic Electronics* **37**
[35] Stoumpos C C *et al* 2015 *J. Am. Chem. Soc.* **137** 21
[36] Chung I *et al* 2016 *Nature* **485** 7399
[37] Kumar M *et al* 2014 *Adv. Mater.* **26** 41
[38] Gupta S *et al* 2016 *ACS Energy Lett.* **1** 5
[39] Sabba D *et al* 2015 *J. Phys. Chem.* C **119** 4
[40] Bhargava P *et al* 2016 *RSC Advances* **6** 19857
[41] Moghe D *et al* 2016 *Nano Energy*, **28**
[42] Huang J Y *et al* 2009 *Jap. Jour. Appl. Phys.* **48** 11R
[43] Lin Z-G *et al* 2008 *J. Cryst. Growth* **310** 13
[44] Huang L *et al* 2016 *Phys. Rev.* B **93** 195211
[45] Amat A *et al* 2014 *Nano Lett.* **14** 6
[46] Kieslich G *et al* 2015 *Chem. Sci.* **6** 3430
[47] Blum V *et al* 2009 *Comp. Phys. Commun.* **180** 2175
[48] Perdew J *et al* 1996 *Phys. Rev. Lett.* **77** 18
[49] Heyd J *et al* 2003 *J. Chem. Phys.* **118** 18
[50] Van Lenthe E *et al* 1996 *J. Chem. Phys.* **105** 6505
[51] Becker P *et al* 2019 *Adv. Energy Mater.* 1900555
[52] Beal R E *et al* 2016 *J. Phys. Chem. Lett.* **7** 746
[53] Opahle I *et al* 2012 *Phys. Chem. Chem. Phys.* **14** 16197
[54] Emery A *et al* 2017 *Sci. Data* **4** 170153
[55] Sato T *et al* 2016 *Scientific Reports* **6** 23592
[56] Travis W *et al* 2016 *Chem. Sci.* **7** 4548
[57] Körzdörfer T *et al* 2016 *Organic Semiconductors* (Singapore: World Scientific Publishing Co)
[58] Liu D *et al* 2019 *RSC Adv.* **9** 3279